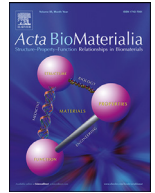




Contents lists available at ScienceDirect

Acta Biomaterialia

journal homepage: www.elsevier.com/locate/actbio

Full length article

Collagenase Type I and Probucol-Loaded Nanoparticles Penetrate the Extracellular Matrix to Target Hepatic Stellate Cells for Hepatic Fibrosis Therapy

Xiaowei Wang^a, Wenjun Zhang^c, Sheng Zeng^b, Liudi Wang^b, Bin Wang^{b,*}^a Department of Biobank, Nanjing Drum Tower Hospital, The Affiliated Hospital of Nanjing University Medical School, Nanjing, Jiangsu, China^b Clinical Stem Cell Center, the Affiliated Drum Tower Hospital of Nanjing University Medical School, Nanjing, Jiangsu Province, China^c Department of Laboratory Medicine, Nanjing Drum Tower Hospital, The Affiliated Hospital of Nanjing University Medical School, Nanjing, China

ARTICLE INFO

Article history:

Received 12 August 2023

Revised 12 December 2023

Accepted 15 December 2023

Available online xxx

Keywords:

Hepatic fibrosis

Hepatic stellate cells

Autophagy

Collagenase type I

Probucol

Drug delivery

ABSTRACT

Hepatic fibrosis is a common pathological process in chronic liver diseases, characterized by excessive reactive oxygen species (ROS), activated hepatic stellate cells (HSCs), and massive synthesis of extracellular matrix (ECM), which are important factors in the development of liver cirrhosis, liver failure, and liver cancer. During the development of hepatic fibrosis, ECM collagen produced by activated HSCs significantly hinders medication delivery to targeted cells and reduces the efficiency of pharmacological therapy. In this study, we designed a multifunctional hyaluronic acid polymeric nanoparticle (HA@PRB/COL NPs) based on autophagy inhibitor probucol (PRB) and collagenase type I (COL) modification, which could enhance ECM degradation and accurately target HSCs through specificity binding CD44 receptor in hepatic fibrosis therapy. Upon encountering excessive collagen I-deposition formed barrier, HA@PRB/COL NPs performed the nanodrill-like function to effectively degrade pericellular collagen I, leading to greater ECM penetration and prominent HSCs internalization capacity of delivered PRB. In mouse hepatic fibrosis model, HA@PRB/COL NPs were efficiently delivered to HSCs through binding CD44 receptor to achieve efficient accumulation in fibrotic liver. Further, we showed that HA@PRB/COL NPs executed the optimal anti-fibrotic activity by inhibiting autophagy and activation of HSCs. In conclusion, our novel dual-functional co-delivery system with degrading fibrotic ECM collagen and targeting activated HSCs exhibits great potentials in the treatment of hepatic fibrosis in clinic.

Statement of significance

The excess release of extracellular matrix (ECM) such as collagen in hepatic fibrosis hinders medication delivery and decreases the efficiency of pharmacological drugs. We aimed to develop a nano-delivery carrier system with protein hydrolyzed surfaces and further encapsulated an autophagy inhibitor (PRB) to enhance fibrosis-related ECM degradation-penetration and hepatic stellate cells (HSCs) targeting in hepatic fibrosis niche (HA@PRB/COL NPs). The COL of HA@PRB/COL NPs successfully worked as a scavenger to promote the digestion of the ECM collagen I barrier for deeper penetration into fibroid liver tissue. It also accurately targeted HSCs through specifically binding to the CD44 receptor and subsequently released PRB to inhibit autolysosome and ROS generation, thus preventing HSCs activation. Our HA@PRB/COL NPs system provided a promising therapeutic strategy for hepatic fibrosis in a clinic setting.

© 2023 Acta Materialia Inc. Published by Elsevier Ltd. All rights reserved.

1. Introduction

Hepatic fibrosis is an important feature of chronic liver diseases and occurs in almost all forms of liver injury, which promotes disease progression by destroying the normal liver parenchyma [1–3].

Provided that hepatic fibrosis is not treated promptly, it will further deteriorate into liver cirrhosis and/or hepatocellular carcinoma with a high morbidity and mortality rate worldwide [4,5]. Hepatic fibrosis is fundamentally different from cirrhosis in that it could be reversible and remediable with medical therapy [6,7]. Hence, effective treatment strategy for hepatic fibrosis is urgently needed.

Many studies have revealed that hepatic fibrosis is regulated by autophagy as a repair response of chronic liver disease. Autophagy

* Corresponding author.

E-mail address: wangbin022800@126.com (B. Wang).

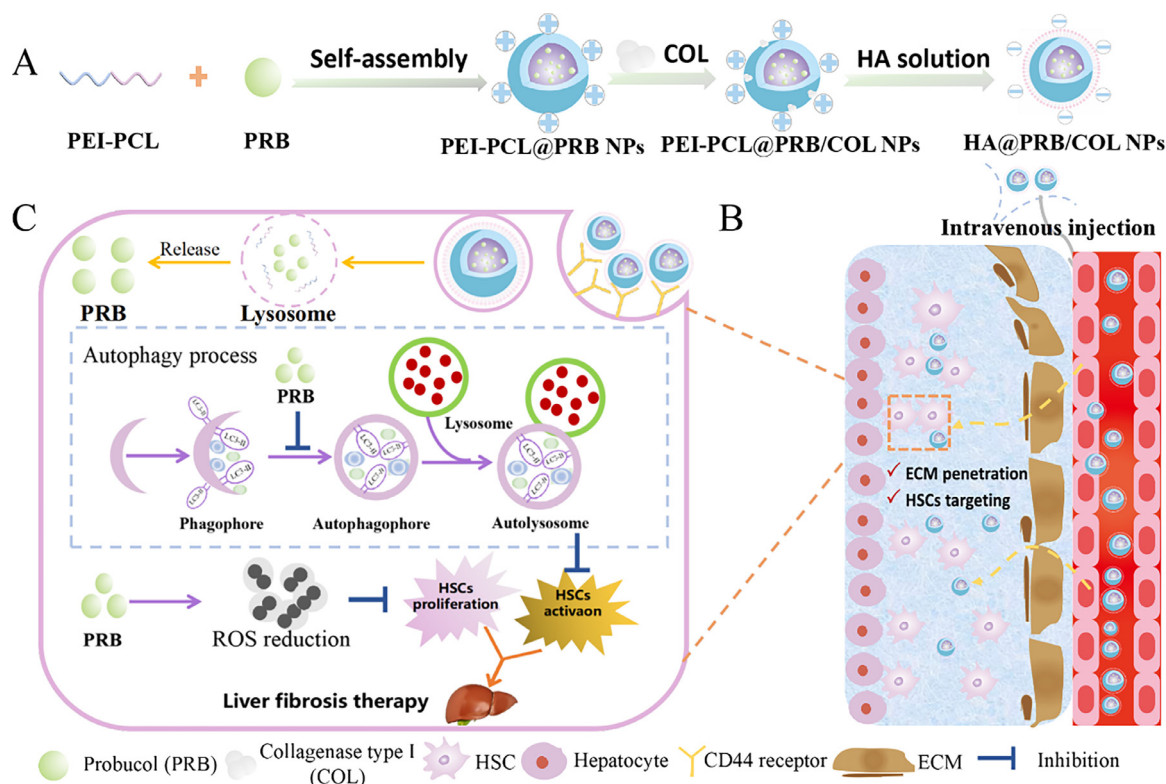


Fig. 1. (A) Schematic illustration of the preparation of HA@PRB/COL NPs. (B) The process of enhancing fibrosis-related ECM degradation-penetration and HSCs targeting on hepatic fibrosis. (C) The mechanism of HA@PRB/COL NP treating hepatic fibrosis by inhibiting autophagy and reducing the generation of ROS.

is a complex metabolic process, which provides energy for HSCs activation by destroying aberrant or useless cytoplasmic components and transports triglycerides, lipid droplets or other components [8,9]. This procedure encourages the conversion of HSCs from a dormant to active state, thereby worsening the hepatic fibrosis [10]. Thus, inhibiting autophagy would be a promising strategy for hepatic fibrosis therapy. Various drugs with the function to block autophagy have been developed [11,12]. For instance, PRB, a conventional hypolipidemic drug, has a considerable anti-lipid oxidation effect and has also been found to have the ability to treat hepatic fibrosis [13,14] by preventing HSCs activation and autophagy [15]. In addition to autophagy, reactive oxygen species (ROS) are also crucial for escalating the inflammatory response, promoting the generation of profibrotic mediators and initiating hepatic fibrosis [16–18]. However, the therapeutic effect of drug does not perform as well in achieving satisfactory therapeutic efficacy due to the lack of targeting the unique hepatic fibrosis environment and effective ECM penetration capability. Besides, non-targeted drug delivery also leads to the uneven distribution of other organs such as the spleen and kidney, impacting their regular physiological functions and severely restricting its clinical application.

In response to numerous chronic liver injuries, HSCs are activated and proliferated, producing excessive ECM proteins and leading to escalating hepatic fibrosis [19–21]. As the main fibrotic effector cells in the pathogenesis of hepatic fibrosis, nanodrug delivery systems targeting the activated HSCs have emerged as a focus of hepatic fibrosis therapy research [22–24]. CD44 receptor is specifically overexpressed on activated HSCs, and some natural substrates such as hyaluronic acid (HA) and chondroitin sulfate (CS) show a high affinity for the CD44 receptor on activated HSCs [25]. HA with good biocompatibility and non-toxicity might be used as a ligand for nano-delivery systems, lessening the harmful side effects of medications for hepatic fibrosis therapy [26–28]. However, it is currently not fully addressed how

to effectively penetrate the ECM barrier of the hepatic fibrosis environment for nano-delivery systems. For targeted drug delivery, current medicines aim to reduce ECM deposition or speed up breaking ECM barrier. Studies had demonstrated that disruption of the ECM collagen barrier by in situ collagenase increases drug penetration in ECM accumulation tissues and boosts therapeutic effectiveness [29–32]. Consequently, aiming to penetrate ECM collagen barrier using a collagenase-modified nano-delivery system is supposed to reinforce the therapeutic efficacy of hepatic fibrosis.

Herein, we developed a nano-delivery carrier with protein hydrolyzed surfaces and further physically encapsulated autophagy inhibitor (PRB) to enhance fibrosis-related ECM degradation-penetration and HSCs targeting on hepatic fibrosis (Fig. 1). A multi-functional amphiphilic nanomaterial (PEI-PCL) was prepared to effectively encapsulate low toxic collagenase type I (COL) through electrostatic attraction and hydrophobic drug probucol by hydrophobic interactions. In order to improve the stability in the blood circulation and the active targeting ability of nanoparticles on activated HSCs, HA is applied to the surface of the nanoparticles to obtain multi-layer nanoparticles (HA@PRB/COL NPs) with multiple functions. After being administered intravenously, the COL of HA@PRB/COL NPs worked as a scavenger to encourage digestion of the ECM collagen I barrier for deeper penetration in fibrotic liver, accurately targeted HSCs through specificity binding CD44 receptor, and released PRB to inhibit autolysosome and ROS generation, thus preventing HSCs activation. The *in vivo* biodistribution of HA@PRB/COL NPs was studied at the level of organs and cells in the CCl₄-induced hepatic fibrosis model. In addition, the antifibrotic activity and fibrotic ECM degradation-penetration efficiency of HA@PRB/COL NPs were systematically analyzed. We hypothesized that the combination of chemotherapeutic and biomacromolecular drugs could provide a promising delivery strategy for the therapy of hepatic fibrosis by facilitating

ECM degradation-penetration and simultaneously decreasing HSCs activation and proliferation.

2. Materials and methods

2.1. Materials

Hyaluronic acid was obtained from Tianjin Xiensi Biochemical Technology Co., Ltd. Polyethyleneimine-polycaprolactone (PEI-PCL, Mn = 5000) was bought from Xi'an Ruixi Biological Co., Ltd. Collagenase type I (COL) was purchased from Hefei Bomei Biotechnology Co., Ltd (Anhui, China). DAPI solution was obtained from Beyotime Biotechnology Co., Ltd (Jiangsu, China). Cell Counting Kit-8 (CCK-8) was purchased from Nanjing Vazyme Biotech Co., Ltd (Jiangsu, China). Probucol (PRB), Lipopolysaccharide (LPS) and Rapamycin (RAP) were provided by Shanghai Aladdin Biochemical Technology Co., Ltd (Shanghai, China).

2.2. Preparation of HA@PRB/COL NPs

PRB and COL were loaded into PEI-PCL by the phacoemulsification and electrostatic adsorption method respectively. In brief, PEI-PCL (3 mg) and PRB (2 mg) were dissolved in CHCl₃ (1 mL), then the solution was treated by ultrasonication and uniformly swirled for 2 min. Subsequently, the solution was slowly dripped (the dripping speed was 2 s/drop) into the 5% glucose solution (5 mL) under the vortex condition to obtain the milky white solution. After the dripping was finished, the solution was sonicated for 10 min to produce a milky white solution. Eventually, the CHCl₃ was removed using rotary evaporation to obtain the white transparent solution (PEI-PCL@PRB NPs). The glucose solution (5%) was applied to dissolve HA and COL. To create PEI-PCL@PRB/COL NPs, PEI-PCL@PRB NPs were first added to the COL solution (1 mg/mL) while being gently stirred. After that, PEI-PCL@PRB/COL NPs (1.0 mL, the concentration of PEI-PCL: 1 mg/mL) was dropped into the HA solution (2.0 mL, the concentration of solution: 2 mg/mL) at room temperature to create HA@PRB/COL NPs. Unencapsulated drug was extracted through using ultrafiltration method (MWCO 3500 Da, 5000 r/min, 30 min). The dye coumarin-6 (C6), FITC and DiR encapsulated the nanoparticles were also prepared in the same way. PEG/ PEI-PCL@FITC NPs (PEG @FITC NPs) were prepared by phacoemulsification.

2.3. Characterization of HA@PRB/COL NPs

The morphology of PEI-PCL@PRB/COL NPs and HA@PRB/COL NPs were examined by employing the transmission electron microscope (TEM, JEM-1200EX, Japan) and atomic force microscopy (AFM, MULTIMODE 8/innova, USA). The size distribution, polydispersity index (PDI) and zeta potential measurements of the nanoparticles were evaluated with the Malvern panalytical analyzer (Nano-ZS 90, Malvern, UK). X-ray powder diffraction (XRD) pattern (D/MAX-2500, Rigaku, Japan) was assessed to observe the structure of PRB, HA@PEI-PCL NPs and HA@PRB/COL NPs.

In order to distinguish between HA@PRB NPs, HA@COL NPs and HA@PRB/COL NPs, Fourier transform infrared spectroscopy (FTIR), ¹Hydrogen-nuclear magnetic resonance (¹H-NMR) and UV-visible spectrophotometer were applied.

The drug loading capacity (DLC%) and drug encapsulation efficiency (DEE%) of PRB encapsulated in the nanoparticles were determined by employing the UV spectrophotometer and measured at 242 nm.

$$DEE\% = \frac{\text{weight of encapsulated PRB in the nanoparticles}}{\text{weight of total PRB}}$$

$$DLC\% = \frac{\text{weight of encapsulated PRB in the nanoparticles}}{\text{weight of total nanoparticles}}$$

To assess the biocompatibility, the hemocompatibility of the polymeric nanoparticles was tested *in vitro*. In short, whole blood of male rat was taken, heparinized to prevent coagulation and red blood cells were collected by centrifugation (3000 rpm, 10 min). 200 μL of red blood cells was added to 800 μL of different concentrations of HA@PRB/COL NPs (0.2, 0.4, 0.6, 0.8, 1.0 mg/mL), normal saline (the negative control group) and distilled water (the positive control group). After incubation for 4 h at 37 °C, samples were centrifuged at the same speed for 10 min and the OD values of supernatant were measured at 576 nm by UV-visible spectrophotometer. The hemolytic percentage (HD%) was calculated as $[(A_{\text{sample}} - A_{\text{negative}})/(A_{\text{positive}} - A_{\text{negative}})] \times 100\%$, A_{sample} was the absorbance of HA@PRB/COL NPs solution, A_{negative} was the absorbance of normal saline, A_{positive} was the absorbance of distilled water.

In vitro the release profile of PRB from HA@PRB NPs and HA@PRB/COL NPs was examined by dialysis method. In brief, 2 mL of HA@PRB NPs and HA@PRB/COL NPs dispersion were loaded into the dialysis bag (MWCO = 3.5 kDa) and dialyzed in 25 mL pH7.4 PBS solution containing 5% (v/v) ethanol, subsequently incubated at 37°C with gentle shaking (100 rpm). Meanwhile, PRB was co-dissolved in DMSO to form the free drug solution and put it into the dialysis bag. At pre-determined time points, 2ml of culture solution was sampled and replaced with 2 mL of freshly released culture solution. The release of PRB was determined by the UV-visible spectrophotometer.

2.4. Cell culture

The L02 human hepatocyte cell line was obtained from Wuhan Shangen Biotechnology Co., Ltd (Wuhan, China). The LX2 human hepatic stellate cell line was purchased from the Cell Bank of Chinese Academy of Sciences (Shanghai, China). L02 and LX2 cells were cultured in DMEM supplemented with 10% (v/v) FBS, 100 μg/mL streptomycin and 100 U/mL penicillin at 37°C in a humidified 5% CO₂ atmosphere.

2.5. Cellular uptake and intracellular trafficking

L02 and LX2 cells were seeded in confocal dishes at an initial density of 8000 cells/well and allowed to grow for 24 h. Then the culture medium was discarded and replaced by FBS-free medium with free FITC, PEG@ FITC NPs, HA@FITC NPs (FITC concentration, 0.025 μg/well). To investigate the competitive behavior of CD44 receptors, LX2 cells were pre-saturated with HA solution, HA@FITC NPs were then added again for incubation (HA + HA@FITC NPs). After incubating in 37°C darkness for another 4 h, cells were washed with cold PBS and stained for 10 min with DAPI. Finally, the samples were visualized thorough confocal laser scanning microscopy (CLSM).

To quantify the intracellular fluorescence intensity of free FITC, PEG@ FITC NPs, HA@FITC NPs by flow cytometry. L02 and LX2 cells were seeded into 12-well plates (1 × 10⁵ cells per well) and incubated for 24 h. Then cells were treated with free FITC, PEG@ FITC NPs, HA@FITC NPs solution. After 4 h incubation, cells were washed three times with PBS, trypsinized, centrifuged at 1500 rpm for 3 min, collected and suspended in PBS. The mean fluorescence intensity of FITC was measured by flow cytometry (BD FACSCelesta, USA).

For intracellular trafficking study of HA@FITC NPs, LX2 cells were seeded in confocal dishes and incubated for 24 h. Then cells were treated with HA@FITC NPs solution. After 0, 2, 4, 6 h incubation, cells were washed three times with PBS and stained with lyso-tracker red for 1 h according to the protocol. Moreover, LX2 cells were incubated with HA@FITC NPs for 2 h, and then endoplasmic reticulum (ER) marker or Golgi marker were added sepa-

rately for 30 min before the cells were washed. After incubation, the cells were washed three times again with PBS and stained for 10 min with DAPI. Ultimately, the wells were imaged by CLSM.

2.6. Cellular uptake in the presence of collagen I barrier

The polycarbonate membrane of Transwell chambers was uniformly coated with a collagen suspension according to the manufacturer's instructions to form the collagen I layer. LX2 cells were seeded in 24-well plates (5×10^4 cells/well) and grew for 24 h. After that, the upper layer of collagen I in the Transwell chamber was then covered with 200 μ L of FBS-free medium containing free C6, HA@C6 NPs, and HA@C6/COL NPs (C6 concentration, 0.025 μ g/mL). LX2 cells were cultured for 1 and 6 h at 37°C in the dark. After incubation, cells were washed three times with PBS, trypsinized, centrifuged at 1500 rpm for 3 min, collected and suspended in PBS, flow cytometry was used to determine the mean fluorescence intensity in the LX2 cells.

2.7 Cell proliferation and toxicity

The cell cytotoxicity of different formulation nanoparticles was measured by the CCK-8 assay *in vitro*. LX2 and L02 cells in the logarithmic growth phase were seeded into 96-well culture plates at a density of 5000 cells per well and incubated for 24 h. After growing by static adherence, the original culture medium was sucked out and disposed with free drug (COL and PRB solution), various different formulation nanoparticles or blank nanoparticles at a series of concentrations for another 24 h or 48 h. Finally, the cells were incubated with 100 μ L fresh medium of 10 μ L CCK-8 for 2 h and measured at 450 nm by using a microplate reader.

2.8. Cell apoptosis

The flow cytometry method was applied to study *in vitro* apoptosis induction, LX2 and L02 cells were seeded in a 6-well plate (3×10^5 cells/well) and cultured overnight. The cells were incubated with different formulation nanoparticles for 24 h, followed by collecting suspended in buffer, staining by Annexin V-FITC and PI apoptosis detection kit and assaying with flow cytometry to quantify the level of cell apoptosis (BD FACS Calibur, BD Biosciences, CA, USA).

2.9. Acridine orange stain observing LX2 cells autophagy

To investigate the ability of different formulation nanoparticles to suppress autophagy *in vitro*, LX2 cells were seeded into 6-well cell culture plates (1×10^6 cells/well) and incubated with free drug, HA@COL NPs, HA@PRB NPs and HA@PRB/COL NPs for 24 h, respectively. The level of autophagy was increased by RAP. After incubation, LX2 cells were stained by acridine orange (AO) and imaged using THUNDER Imaging Systems.

2.10. Hepatic fibrosis inhibition in vitro by ROS reduction

To investigate the mechanism of PRB inhibiting hepatic fibrosis. LX2 cells were seeded into 6-well cell culture plates (5×10^5 cells/well) and incubated with free drug, HA@COL NPs, HA@PRB NPs and HA@PRB/COL NPs for 24 h, respectively. The amount of total ROS level within the cell was raised using LPS. After incubation, LX2 cells were stained by 2',7'-dichlorodihydrofluorescein diacetate (DCFH-DA) for 30 min and imaged using THUNDER Imaging Systems. Intracellular ROS levels were quantified by flow cytometry.

2.10. TEM imaging of autophagosomes in LX2 cells

RAP and RAP + HA@PRB/COL NPs were applied to LX2 cells seeded into 6-well cell culture plates (1×10^6 cells/well) for 24 h. Following treatment, the cells were harvested, washed with PBS, and centrifuged to yield cell pellets. After that, 2.5% glutaraldehyde was applied to fix the cell pellets for 24 h at 4 °C, the glutaraldehyde solution was removed and 2% osmium tetroxide was added for another 30 min. Finally, ultrathin sections of LX2 cell pellets were observed using bio-transmission electron microscopy (bio-TEM).

2.11. Immunofluorescence staining of α -SMA and collagen I in vitro

LX2 cells were seeded into 6-well cell culture plates (5×10^5 cells/well) and treated with various formulation nanoparticles for 24 h, afterwards washed and fixed for 20 min with 4 % paraformaldehyde. Thereafter, the cells were then given three PBS washes before being exposed to 0.5% Triton X-100 for 20 min at room temperature. The cells were incubated for 30 min with blocking buffer (5% bovine serum albumin) to reduce nonspecific staining. Then after removing the blocking buffer and washing three times with PBS, the cells were incubated overnight at 4 °C with a rabbit anti-human α -SMA antibody (Cell Signaling Technology, USA) or collagen I primary antibody (Absin, China) diluted in blocking buffer, respectively. Subsequently, cells were then washed three times with PBST and incubated for 2 h at room temperature with Cy3-conjugated goat anti-rabbit secondary antibody (Invitrogen, Shanghai, China). Thereafter, cells were washed three times with PBST and DAPI-containing sealing agent was used to counterstain the nuclei. Finally, cell fluorescence was analyzed using the THUNDER Imaging Systems (Leica, Germany).

2.12. Western blot

The expressions of collagen I, α -SMA, LC3B, p62, connective tissue growth factor (CTGF) and transforming growth factor- β 1 (TGF- β 1) in LX2 cells after treatment were assessed using the western blot method. LX2 cells were harvested and lysed in cold RIPA buffer (Beyotime P0013B), the total protein concentration of cell lysate was determined by bicinchoninic acid assay (Beyotime, P0010). Thereafter, 50 μ g proteins were fractionated on 10% SDS-polyacrylamide gel electrophoresis (SDS-PAGE) and blotted to polyvinylidene fluoride membrane (PVDF, 0.45 μ m) membranes. Afterwards blots were incubated with different primary antibodies overnight at 4 °C, washed three times with PBST and corresponded HRP-conjugated secondary antibodies for 2 h at room temperature. Finally, the PVDF membranes were observed by the supersensitive ECL system (Amersham) and quantified by densitometry using ImageJ software.

2.14. Induction of a mice hepatic fibrosis model

Eight-week-old female C57BL/6 mice (20 ± 2 g) in the same background were obtained from Beijing Vitonglihua Experimental Animal Technology Co., Ltd (Beijing, China). All animal experiments were conducted in accordance with the Guides for the Care and Use of Laboratory Animals from the National Institutes of Health. The animal experiments were approved by the Research Ethics Board of Nanjing Drum Tower Hospital, the Affiliated Hospital of Nanjing University Medical School.

The hepatic fibrosis mice model were induced by intraperitoneal injected with 150 μ L mixture of corn oil and CCl₄ (corn oil: CCl₄ = 3 : 1) twice a week, during an eight-week period. Mice in the untreated group were given the same volume of corn oil as

healthy controls. After 8 weeks, the hepatic fibrosis mice were verified by pathological analysis.

2.15. In vivo biodistribution studies

Fibrotic mice and normal mice were randomly divided into three groups, respectively. Free DiR, HA@DiR NPs or HA@DiR/COL NPs (DiR dosage, 1 mg/kg) were intravenously injected into fibrotic mice and normal mice. Mice were sedated with isoflurane at 6 h, 12 h, and 1, 3, and 5 d following injection, and an *in vivo* imaging system (AniView Kirin, China) was used to conduct fluorescence imaging. On the last day, mice were sacrificed, livers, lungs, spleens, and kidneys were removed for *ex vivo* imaging using the same system and settings as above.

2.16. In vivo HSCs targeting efficiency

The efficiency of HA@PRB/COL NPs targeting HSCs in mice with hepatic fibrosis was analyzed by tissue immunofluorescence assay. The fibrotic mice were treated with free FITC, HA@FITC NPs and HA@FITC/COL NPs. The mice were sacrificed at 24 h after the final injection, the livers were collected and sliced, and the slices were incubated with rabbit anti-mouse α -SMA antibody and goat anti-rabbit secondary antibody conjugated to Cy3. Thereafter, the slices were washed three times with PBST and DAPI-containing sealing agent was used to counterstain the nuclei. Finally, the fluorescence was analyzed using the CLSM (Leica, Germany).

The fibrotic mice were treated with free FITC, HA@FITC NPs and HA@FITC/COL NPs, mice were intravenously treated with HA solution (10 mg/kg) to pre-saturate the CD44 receptor. The same method was used in mice after administration. The slices were incubated with rabbit anti-mouse CD44 antibody and goat anti-rabbit secondary antibody conjugated to Cy3. Finally, the localization was observed using the CLSM (Leica, Germany).

2.17. In vivo anti-hepatic fibrosis therapeutic efficacy

The fibrotic mice were randomly divided into six groups ($n = 5$), whereafter various formulations were administered intravenously twice a week for 3 weeks (PRB dosage, 10 mg/kg). The fibrosis model group and the healthy control group were given the same amount of normal saline through the tail vein. Three days after the last injection, blood was drawn to assess the serum cytokines. Mice were then sacrificed, major organs were removed and stored in 4 % paraformaldehyde for subsequent histological analysis.

2.18. Serum cytokine and hydroxyproline measurements

An AU480 Chemistry Analyzer (Beckman Coulter, IN, USA) was applied to measure the serum levels of alanine aminotransferase (ALT), aspartate aminotransferase (AST), and alkaline phosphatase (ALP) according to reference procedures.

Hydroxyproline (Hyp) content was measured using hydroxyproline assay kit (Jiancheng Biotech) according to the manufacturer's instructions.

2.19. Histopathology assays

Mice major tissues (heart, liver, spleen, lung and kidney) were formalin-fixed and paraffin-embedded for hematoxylin and eosin (H&E) staining. Paraffin-embedded liver tissues were sectioned with 5 μ m. Liver tissue slices firstly were dewaxed by xylene and alcohol, then corresponding steps were carried out according to Masson's trichrome staining Kit (Baso, BA4079A). Furthermore, liver tissue slices were stained Sirius Red according to Picro Sirius Red Stain Kit (PHYGENE, PH1099).

2.20. Statistical analysis

All data in this study was presented as means \pm standard deviation (SD). The two-tailed Student's t-test was applied to analyze the difference between two groups. * $p < 0.05$, ** $p < 0.01$ and *** $p < 0.001$ were considered as statistically significant.

3. Results and discussion

3.1. Characterization of polymeric nanoparticles

In this study, polymeric nanoparticles were prepared using the phacoemulsification and electrostatic adsorption procedure. The HA shell was encapsulated on the nanoparticles surface by electric charging attraction (Fig. 1A). As in listed Fig. 2A and Table 1, the zeta potential of nanoparticles rapidly decreased as the mass ratio of HA to PEI-PCL rose. The mass ratio of HA and PEI-PCL was ultimately selected at 4:1 as the formulation of the subsequent polymeric nanoparticles. The average size of HA@PRB NPs, HA@COL NPs, and HA@PRB/COL NPs was 142.5 ± 7.6 , 146.7 ± 13.2 , and 147.1 ± 8.4 nm, respectively. The zeta potential values of HA@PRB NPs, HA@COL NPs, and HA@PRB/COL NPs exhibited -12.7 ± 0.5 , -13.4 ± 0.2 and -13.7 ± 0.3 mV, respectively. Polymeric nanoparticles were shielded from cationic proteins in plasma during blood circulation, otherwise they would be eliminated. The DEE% of PRB and COL were 82.4 ± 4.7 % and 83.6 ± 3.7 %, and the DLC% of PRB and COL were 24.7 ± 1.7 % and 14.8 ± 0.7 %, respectively.

To demonstrate the structure of HA@PRB NPs, HA@COL NPs, and HA@PRB/COL NPs, $^1\text{H-NMR}$, FTIR spectroscopy and UV-visible spectrophotometer were used. The typical $^1\text{H-NMR}$ spectrum indicated that the peaks located at $\delta = 1.10 - 1.50$ ppm were the displacement of hydrogen at the terminal methylene and intermediate methylene, respectively. $\delta = 5.30$ ppm was the characteristic hydrogen in the PRB structure (Figure.S1). The FTIR spectrum demonstrated two broad peaks at $3,300 - 3,600 \text{ cm}^{-1}$, belonging to the O-H and N-H bands of the polymer and drug. The peaks at $1,508 - 1,669 \text{ cm}^{-1}$ were characteristic bands of NH primary bending and NH secondary bending vibrations of the polymer. An intense peak at $600 - 900 \text{ cm}^{-1}$ was the characteristic esoteric (C-C) bands of drug (Figure.S2). The UV absorption wavelengths of PRB and HA were at 242 nm and 280 nm, respectively (Figure.S3). Combined with the XRD pattern (Fig. 2B), the disappearance of PRB crystal peaks indicated that PRB was encapsulated in the nanoparticles with an amorphous state. The results indicated that PRB and COL had been successfully combined with HA@PRB/COL NPs.

Furthermore, PEI-PCL@PRB/COL NPs and HA@PRB/COL NPs indicated uniformly dispersed spherical morphologies in TEM images (Fig. 2C and 2D). AFM was also applied to characterize the morphology, the formulations of HA@PRB NPs, HA@COL NPs, and HA@PRB/COL NPs were spherical shape (Figure.S4).

In order to evaluate the biocompatibility of HA@PRB/COL NPs, hemolytic activity was studied. HA@PRB/COL nanoparticles had no obvious hemolytic activity and had good blood compatibility (Fig. 2E). The size and zeta potential of the particles did not change appreciably, and at the same time no drug leakage occurred for up to 72 h in pH 7.4 PBS and 10% FBS. The results suggested that HA@PRB/COL NPs should have strong structural stability throughout blood circulation (Fig. 2F and Figure.S5).

As indicated in Fig. 2G, the free PRB solution showed a burst release of about 80 % of the PRB within 24 h. In contrast, the relative cumulative release of PRB from HA@PRB NPs and HA@PRB/COL NPs exhibited no more than 45 % within 24 h, suggesting that the polymeric nanoparticles followed sustained-release manners. The slow-release properties might ensure effective accumulation of PRB into

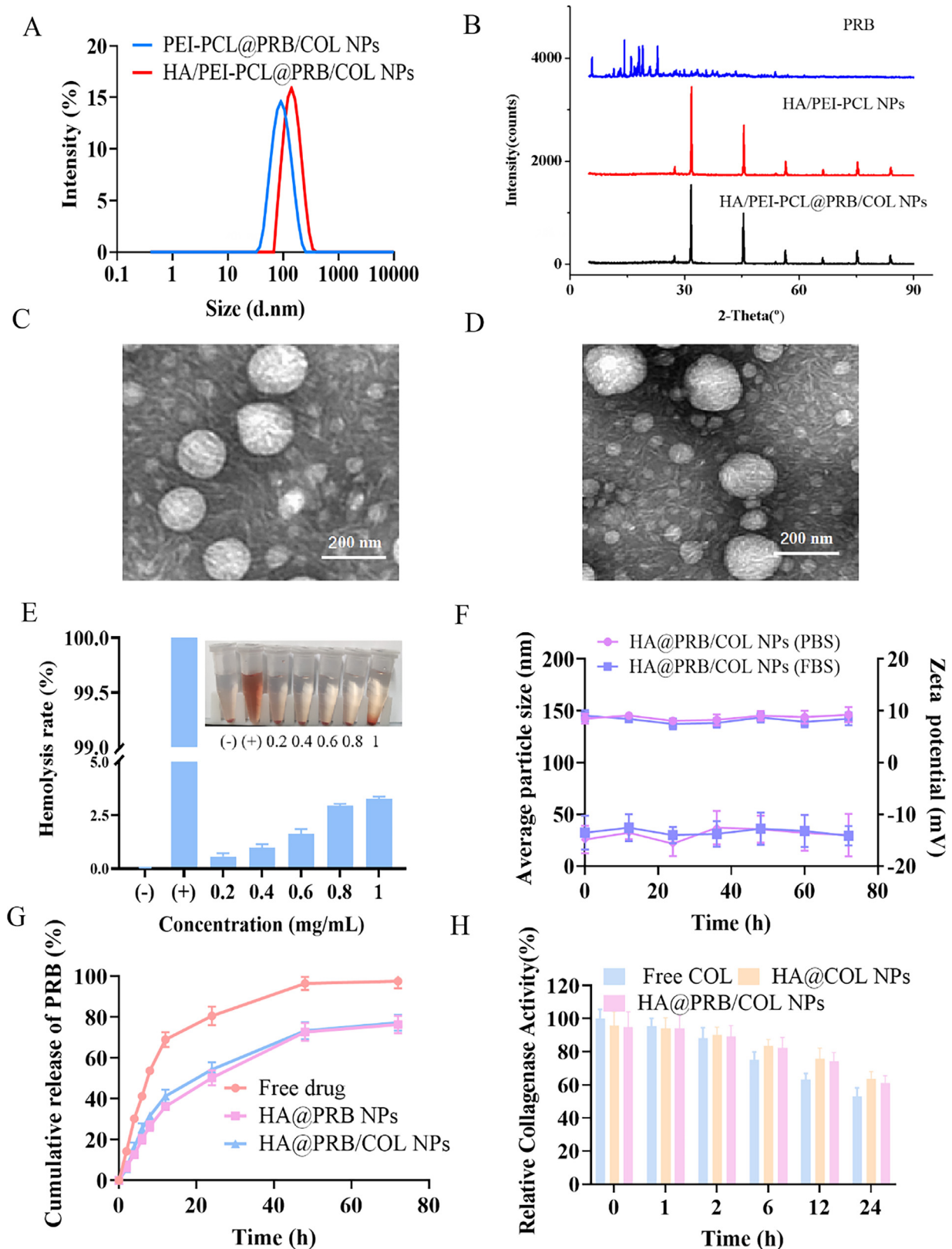


Fig. 2. Characterization of polymeric nanoparticles. (A) Size distribution of PEI-PCL@PRB/COL NPs and HA/PEI-PCL@PRB/COL NPs. (B) XRD diffraction analysis of PRB, HA/PEI-PCL NPs and HA/PEI-PCL@PRB/COL NPs. (C) TEM images of PEI-PCL@PRB/COL NPs. (D) TEM images of HA@PRB/COL NPs. (E) Hemolytic analysis of HA@PRB/COL NPs at different concentrations. (F) Size and zeta potential change of HA@PRB/COL NPs in PBS and FBS. (G) *In vitro* PRB release profiles. (H) The enzyme activity of HA@COL NPs, HA@PRB/COL NPs and free COL solution at different incubation time points. Values are expressed as means \pm SD ($n = 3$).

Table 1

Characterization of various formulation polymeric nanoparticles.

Formulations	Mass ratio (HA/PEI-PCL)	Size (nm)	PDI	Zeta potential (mV)	DEE (%)	DLC (%)
PEI-PCL NPs	–	89.6 ± 5.7	0.136	27.6 ± 0.2	–	–
HA/PEI-PCL NPs	2/1	123.4 ± 8.6	0.154	–8.9 ± 0.1	–	–
	4/1	125.7 ± 11.2	0.158	–12.7 ± 0.3	–	–
	6/1	125.7 ± 11.2	0.156	–13.7 ± 0.3	–	–
PEI-PCL@PRB/COL NPs	–	106.6 ± 8.2	0.169	17.8 ± 0.6	–	–
HA/PEI-PCL@PRB NPs (HA@PRB NPs)	4/1	142.5 ± 7.6	0.154	–12.7 ± 0.5	85.6 ± 4.4	19.7 ± 1.3
HA/PEI-PCL@COL NPs (HA@COL NPs)	4/1	146.7 ± 13.2	0.176	–13.4 ± 0.2	81.6 ± 5.6	12.5 ± 0.9
HA/PEI-PCL@PRB/COL NPs (HA@PRB/COL NPs)	4/1	147.1 ± 8.4	0.164	–13.7 ± 0.3	82.4 ± 4.7	24.7 ± 1.7
					83.6 ± 3.7	14.8 ± 0.7

the fibrotic liver after blood circulation, which is critical for lasting therapeutic efficacy of hepatic fibrosis.

So as to avoid denaturation of the COL during the loading process, no organic reagents were employed in the preparation of the nanoparticles. Additionally, COL was encapsulated based on electrostatic attraction rather than chemical interactions to avoid denaturation and guarantee release rates at target areas. Measurements of the *in vitro* enzyme activity revealed that the enzyme activity remained after COL coated on HA@COL NPs and HA@PRB/COL NPs, the enzyme activity was approximately 90 % (Fig. 2H). This result indicated that the enzyme activity was not significantly affected by the preparation technique. The enzyme activity of HA@COL NPs and HA@PRB/COL NPs gradually decreased over the course of an extended incubation period and it remained above 50% after 24 h, which indicated slightly higher enzyme activity and maintained enzyme activity levels for a longer period of time compared to COL solution *in vitro*.

3.2. Cellular uptake and intracellular distribution *in vitro*

A cell surface glycoprotein called CD44 is involved in migration, adhesion, and interactions between cells. The activation and proliferation of HSCs is accompanied by the overexpression of CD44 receptors on their surface, which contributes to hepatic fibrosis. The expression level of the CD44 receptors on the HSCs (LX2 cells line) is significantly higher than on normal hepatocyte (L02 cells line). Modification of hyaluronic acid onto nanoparticles could enhance the affinity for CD44 receptors and improve cellular uptake of HSCs. FITC was applied to detect nanoparticles uptake in LX2 cells and L02 cells. After incubation of both cell types with all groups for 4 h, the FITC fluorescence signals of all groups were mainly observed in the cytoplasm (Fig. 3A). Compared with PEG@FITC NPs and the FITC solution, HA@FITC NPs had the maximum fluorescence intensity in LX2 cells, demonstrating that HA@FITC NPs efficiently increased FITC transport into LX2 cells. In comparison, LX2 cells showed greater amounts of intracellular HA@FITC NPs than L02 cells and there was no significant difference in fluorescence signals in L02 cells among all groups (Fig. 3D).

The competitive uptake of HA@FITC NPs by CD44 receptor was further studied. As shown in Fig. 3A, the relevance of HA-dependent CD44 receptor-mediated endocytosis was demonstrated, this competitive interaction of CD44 receptors decreased the internalization content of HA@FITC NPs when HA solution was utilized to pre-saturate the CD44 receptors on the surface of HSCs. At the same time, we quantitatively studied the uptake of two kinds of cells by flow cytometry. On the LX2 cells, the average fluorescence intensity of HA@FITC NPs was higher than L02 cells (Fig. 3B and 3C, Fig. 3E and 3F). The quantitative analysis of intracellular uptake efficiency by flow cytometry was consistent with CLSM.

Confocal microscopy demonstrated that HA@FITC NPs internalized in LX2 cells over a period of time (Fig. 3G). Lysosomes and cell nuclei were labeled with lyso-tracker red and DAPI, respectively. After incubating for 2 h and 4 h, lyso-tracker red and FITC fluorescence (green) colocalization mainly derived from late endosomes and lysosomes. The ER and Golgi were stained after 2 h of incubation, and a small number of nanoparticles were present in the ER and Golgi (Figure.S6), this result further suggested that HA@FITC NPs internalization were transported via the endolysosomal route in LX2 cells. Moreover, the fluorescence signal of HA@FITC NPs increased significantly with the extension of incubation time, the green fluorescence gradually did not colocalization with red fluorescence and the green fluorescence was widely distributed in cells after 6 h of incubation, indicating HA@FITC NPs could escape from the lysosome, so that the released drug escaped from the acidic endosome/lysosome into the cytoplasm. These results confirmed the intracellular process of polymeric nanoparticles for better therapeutic efficacies.

3.3. *In vitro* fibrotic ECM degradation activity

One of the key elements of the ECM in the fibrotic liver is collagen I. In Transwell chambers, collagen I was pre-layered over polycarbonate membrane to create an ECM barrier. In order to assess the degradation-penetration ability of polymeric nanoparticles *in vitro*, flow cytometry was used to measure the uptake of all groups in LX2 cells at 1 and 6 h after adding free C6 or various C6 loaded polymeric nanoparticles to the upper Transwell chambers (Fig. 4A). In LX2 cells at 1 and 6 h, the quantitative results showed no discernible difference in intracellular accumulation between free C6 and HA@C6 NPs, proving that a large amount collagen I acted as a barrier to polymeric nanoparticles entry (Fig. 4B). In contrast, HA@C6/COL NPs effectively penetrated the ECM barrier and HA@C6/COL NPs were accessible into the lower cell culture medium and internalized by HSCs. Compared with free C6 and HA@C6 NPs, HA@C6/COL NPs treated for 6 h increased the fluorescence intensity about 5.5 and 4.5 folds, respectively. The results indicated that the presence of collagenase I on the surface of polymeric nanoparticles significantly promoted the penetration of collagen I barrier.

3.4. *In vitro* cell viability and proliferation inhibition

The activation and proliferation of HSCs is the primary stage in the development of hepatic fibrosis. The viability of LX2 cells and L02 cells incubated with different concentrations of drug-free polymeric nanoparticles, free drug, HA@PRB NPs, HA@COL NPs and HA@PRB/COL NPs for 24 h and 48 h was evaluated by CCK-8 assay. After 48 h of incubation, the survival of drug-free polymeric nanoparticle was higher than 90% for LX2 cells and L02 cells at polymeric nanoparticle concentrations below 50 µg/mL, indicating

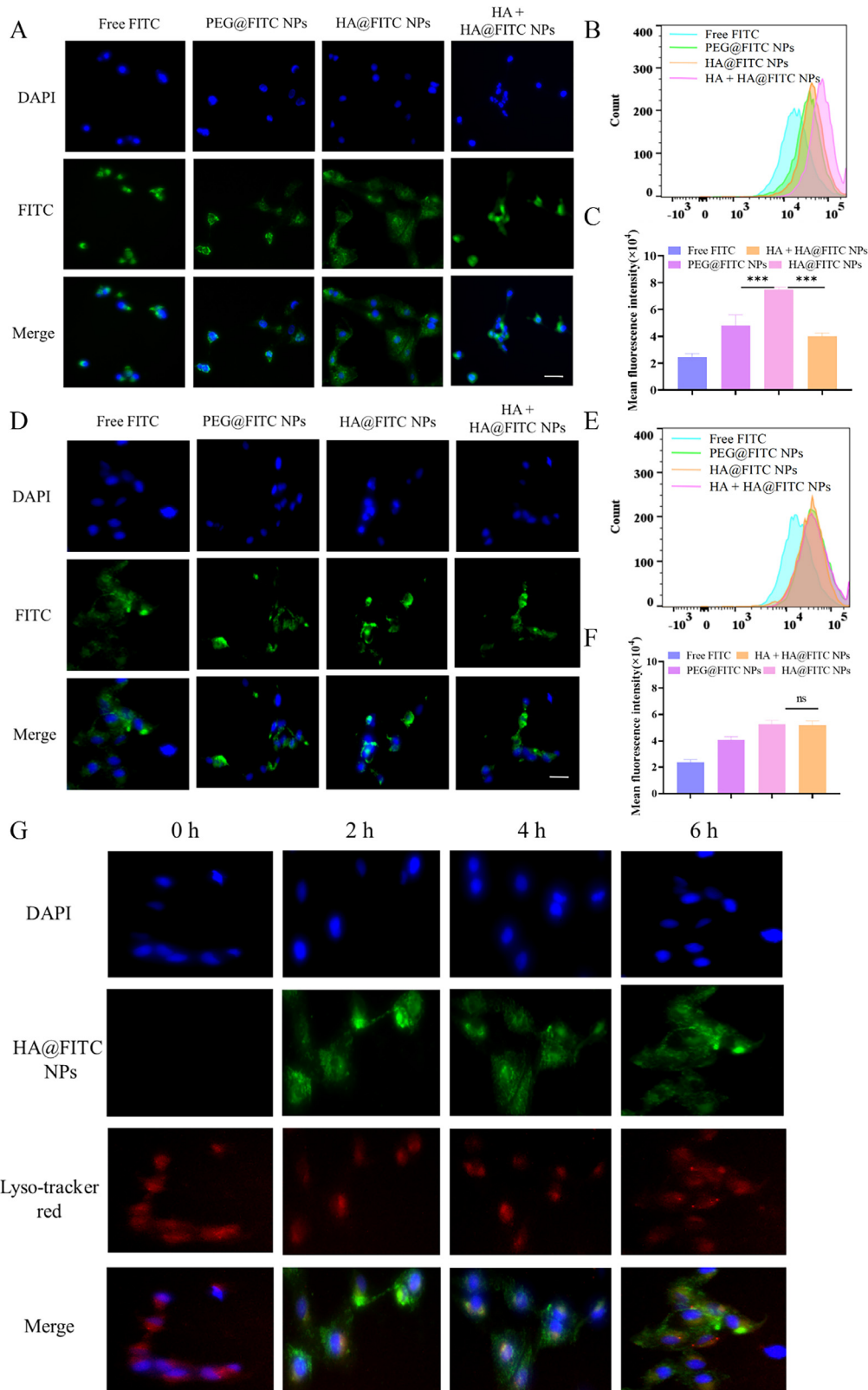


Fig. 3. Cellular uptake of polymeric nanoparticles *in vitro*. (A) Intracellular uptake of free FITC, PEG@ FITC NPs and HA@ FITC NPs in LX2 cells and HA pre-saturated HSCs presented as the CLSM image after incubation for 4 h, respectively. Scale bar = 50 μ m. (B) The flow cytometry after incubation with different formulations for 4 h in LX2 cells. (C) The quantitative of flow cytometry histograms after incubation with different formulations for 4 h in LX2 cells. (D) Intracellular uptake of free FITC, PEG@ FITC NPs and HA@ FITC NPs in L02 cells presented as the CLSM image after incubation for 4 h, respectively. Scale bar = 50 μ m. (E) The flow cytometry after incubation with different formulations for 4 h in L02 cells. (F) The quantitative of flow cytometry histograms after incubation with different formulations for 4 h in L02 cells. *** $p < 0.001$, and ns means no significant difference. (G) Intracellular trafficking analysis. LX2 cells were incubated with HA@FITC NPs at different times; a lysosome marker was added before the cells were washed; the cells were imaged using confocal microscopy. Scale bar = 50 μ m.

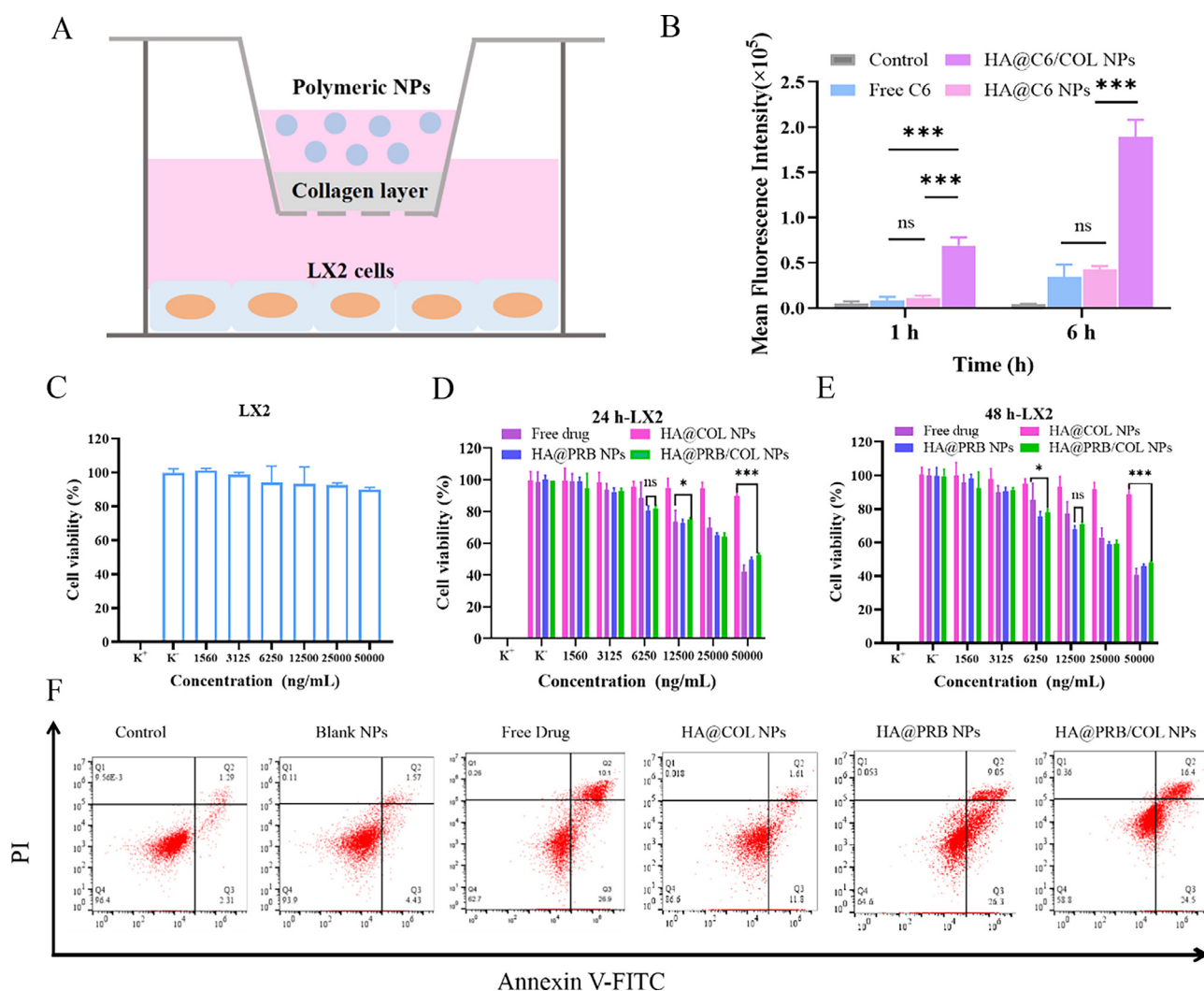


Fig. 4. Cellular uptake of polymeric nanoparticles through anti-collagen I barrier activity and therapeutic effect of HA@PRB/COL NPs *in vitro*. (A) Illustration of the *in vitro* collagen I barrier model. (B) The flow cytometry histogram in LX2 cells 1 and 6 h after adding free C6 or different C6-loaded polymeric nanoparticles to Transwell chambers ($n = 3$). (C) Cell viability of LX2 cells treated with drug-free polymeric nanoparticles at different concentrations. (D) Cell viability profiles of LX2 cells treated with various formulations for 24 h. (E) Cell viability profiles of LX2 cells treated with various formulations for 48 h. *** $p < 0.001$; ns, no significant difference ($n = 3$, mean \pm SD). (F) Flow cytometry analysis of the apoptosis of LX2 cells after different treatments.

that drug-free polymeric nanoparticles had good biocompatibility at these concentrations (Fig. 4C and Figure.S7). More importantly, the activity of LX2 cells decreased significantly with the increase of PRB concentration (Fig. 4D and 4E). The main reason for the reduced cell viability of free drug might be the rapid passive diffusion of the molecular form. However, compared with the LX2 cells, the L02 cells viability was higher than LX2 cells at the same dose (Figure.S8), demonstrating that the polymer nanoparticles had inhibitory effect on LX2 cells without causing considerable toxicity to normal hepatocytes, promoting the therapy of hepatic fibrosis and reducing adverse effects.

The cell cytotoxicity of the polymeric nanoparticles was analyzed by flow cytometry and the quantitative measurement of apoptosis rate under different treatment groups were presented in Fig. 4F and Figure.S9. Compared with L02 cells, the apoptosis rate of LX2 cells was significantly increased, indicating that HA@PRB/COL NPs had a tendency to destroy LX2 cells and showed the outstanding biocompatible capacity. In addition, HA@PRB/COL NPs significantly increased the number of apoptotic cells (40.9 %) than HA@PRB NPs and HA@COL NPs, HA@PRB/COL NPs had the ability to inhibit the proliferation of HSCs. Therefore, the apoptotic results were consistent with the cytotoxic results.

3.5. Anti-hepatic fibrosis activity and ECM degradation ability *in vitro*

α -SMA is one of the recognition proteins in activated HSCs, and its expression level partially reflects the degree of fibrosis. Based on α -SMA immunofluorescence results and western blot (Fig. 5A and 5C), the slight inhibition of α -SMA in LX2 by HA@COL NPs suggested that COL had a direct effect on collagen I degradation but did not dominate anti-LX2 activation. In stark contrast, the α -SMA signals significantly diminished with the administration of free drug and HA@PRB/COL NPs, indicating that the RRB significantly reduced the activation and proliferation of LX2.

Dynamic collagen is involved in normal tissue development through variations in collagen synthesis and breakdown. Because activated HSCs are one of the main collagen makers in hepatic fibrosis, an imbalance in the dynamic collagen reshaping process could result in anomalies in the structure and metabolism of collagen. Collagen I immunofluorescence results were shown in Fig. 5B, the fluorescence of HA@PRB NPs was stronger than HA@COL NPs and HA@PRB/COL NPs, collagen breakdown of the ECM was partially mediated by COL. Additionally, the western blot results

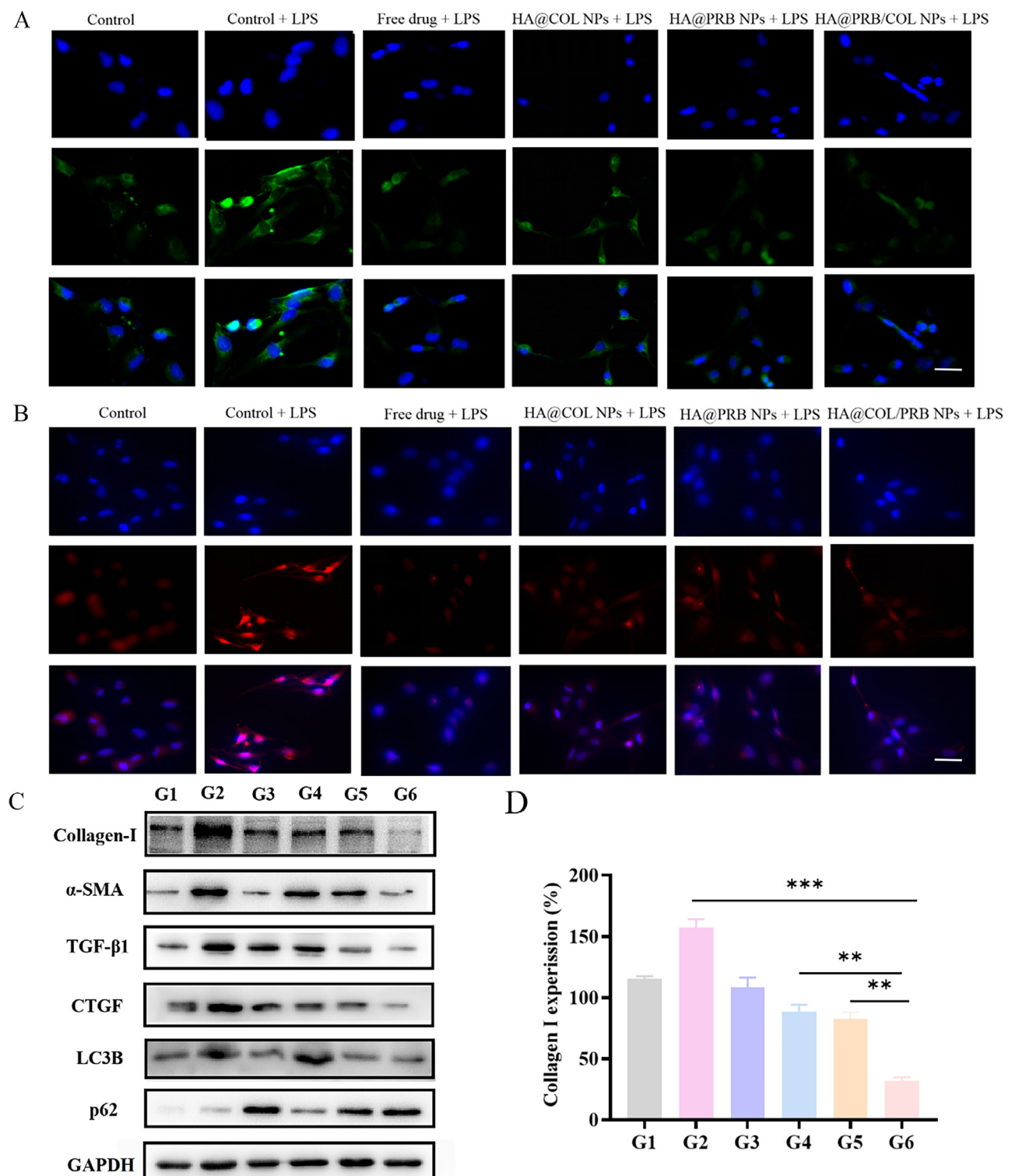


Fig. 5. *In vitro* anti-hepatic fibrosis activity and ECM degradation ability of HA@PRB/COL NPs. (A) α -SMA immunofluorescence stainings of LX2 cells with various formulation treatments. Scale bar = 50 μ m. (B) Collagen I immunofluorescence stainings of LX2 cells with various formulation treatments. Scale bar = 50 μ m. (C) α -SMA, Collagen I, TGF- β 1, CTGF, LC3B and p62 expression in HSCs assayed by western blot, GAPDH was included as loading control. (D) Quantitative analysis of collagen I in LX2. Data are mean \pm SD (n = 3). ** p < 0.01 and *** p < 0.001. (G1: control, G2: control + LPS, G3: free drug + LPS, G4: HA@COL NPs + LPS, G5: HA@PRB NPs + LPS, G6: HA@PRB/COL NPs + LPS).

(Fig. 5C and 5D) matched the immunofluorescence staining of collagen I.

3.6. The mechanism of inhibiting HSCs proliferation and activation

3.6.1. Molecular mechanisms

The most important cytokine in hepatic fibrosis is TGF- β 1, and when the expression level of TGF- β 1 is increased, it promotes the activation of fibroblasts and the transformation into myofibroblasts, which massively express α -SMA and synthesize excess ECM. Therefore, the expression of TGF- β 1 protein in LX2 cells was also measured by western blot. All formulations showed some inhibition of TGF- β 1 expression (Fig. 5C), which was conducive to inhibit the activation of LX2 and the alleviate of hepatic fibrosis. These findings revealed that the co-delivery of COL and PRB had anti-fibrotic effects *in vitro* and synergistically decreased the expression of collagen I and α -SMA in LX2.

In addition, activated HSCs could produce CTGF, promote the proliferation, migration, adhesion and ECM production of fibroblasts, and induce the production of fibrosis. CTGF may also be a common effect factor downstream of multiple fibrotic signaling pathways, which plays a key role in the occurrence and development of hepatic fibrosis. Therefore, CTGF is called a "general switch" generated by fibrosis in liver disease, CTGF acts as a downstream mediator of TGF- β 1 [33,34]. To explore the molecular mechanism of polymeric nanoparticles in alleviating hepatic fibrosis, we investigated the expression of CTGF by western blot (Fig. 5C). The results showed that free drug, HA@PRB NPs and HA@PRB/COL NPs reduced CTGF expression to a certain extent, which might be an important molecular mechanism of probucol against hepatic fibrosis.

3.6.2. Decreased generation of ROS

One of the pathogenic mechanisms of hepatic fibrosis is excessive ROS generation, which causes an imbalance in redox states and the activation of HSCs. ROS acts on the upstream and downstream of TGF- β pathway. ROS activates latency-associated peptides to promote TGF- β release in the upstream, and also promotes TGF- β secretion in a positive feedback loop. According to the pharmacological action of probucol, probucol has the effect of anti-lipid oxidation, and hepatic fibrosis can be reversed by getting rid of excess ROS. In order to investigate the ROS clearance ability of different formulation nanoparticles *in vitro*, LX2 cells were treated with LPS. Then, free drug, HA@COL NPs, HA@PRB NPs and HA@PRB/COL NPs were each incubated with treated LX2 cells for 24 h, and DCFH-DA was utilized to measure the effectiveness of total ROS clearance. CLSM revealed that LPS-treated LX2 cells displayed intense green fluorescence, probably caused by the accumulation of ROS (Fig. 6A). In contrast, HA@PRB/COL NPs significantly reduced ROS levels from 89% to 66% during flow cytometry in LPS-treated LX2 cells (Fig. 6B). Meanwhile, the results of immunofluorescence and western blot results showed that the level of α -SMA decreased after HA@PRB/COL NPs treatment (Fig. 5A and 5C). In conclusion, these results suggested that HA@PRB/COL NPs effectively inhibited proliferation by scavenging excess ROS in LX2 cells.

3.6.3. Inhibition of autophagy process

It had been reported that autophagy significantly promoted the occurrence of hepatic fibrosis through activating HSCs with donor energy. The complex metabolic process of autophagy converts HSCs from a stationary to an activated state, removes dysfunctional or useless cytoplasmic components, transfers triglycerides, lipid droplets, or other components to provide energy for HSCs activation, and further intensifies hepatic fibrosis [9,10]. Therefore, inhibiting autophagy might be a feasible approach for the treatment

of hepatic fibrosis. Some studies had shown that probucol significantly inhibited the autophagy of HSCs, thereby reducing the degree of hepatic fibrosis. Western blot analysis demonstrated that LC3B involved in autophagosome formation was down-regulated (Fig. 5C), indicating a decrease in autophagosomes. As a receptor, p62 takes part in the breakdown of ubiquitinated proteins and is crucial for the creation of autolysosomes and the interpretation of proteins. Therefore, the absence of phagocytosis results in a large buildup of p62 [35,36]. Alternatively, p62 was increased in the free drug (G3), HA@PRB NPs (G5) and HA@PRB/COL NPs (G6), demonstrating that the binding and ensuing solvation of autophagosomes to lysosomes were prevented. Moreover, α -SMA, TGF- β 1, or collagen I expression were significantly reduced in both HA@PRB NPs and HA@PRB/COL NPs, triggering an endogenous negative feedback regulatory mechanism as a result of autophagy inhibition.

Acridine orange (AO) was used to further study the effect of PRB on pH change of organelles. The lysotropic dye AO is a hallmark of acidic vacuolar organelles, which accumulates in acidic vesicles in a pH-dependent manner. At neutral pH, AO is green fluorescence throughout the cell, while in acidic environments, it is protonated and forms aggregates, emitting bright red fluorescence (mainly in late autophagosomes and autolysosomes). As shown in Fig. 6C, compared to the RAP-treated group (G2) of LX2 cells, the AO red fluorescence intensity was less intense in the HA@PRB/COL NPs-treated group (G6). In addition, bio-TEM was used to assess autophagy flow in LX2 cells stimulated by RAP (Fig. 6D). It can be observed from bio-TEM images that the autophagosome membrane was destroyed and the structure became incomplete in HA@PRB/COL NPs treatment group compared with the RAP group, indicating that PRB could inhibit LX2 cells autophagy and reduced the number of autophagosomes.

3.7. In vivo distribution of DiR-loaded polymeric nanoparticles in normal and fibrotic mice

C57BL/6 mice were intraperitoneally injected with carbon tetrachloride (CCl₄; diluted with corn oil) twice a week for 8 weeks to establish the hepatic fibrosis model (Fig. 7A). As displayed in Figure S10, there was an enhanced accumulation of collagen fibrosis in the tissues of the dissected liver through Sirius red and Masson staining, the results further indicated that the hepatic fibrosis mouse model was successfully constructed. Normal mice and mice with fibrotic liver not only have different degrees of fibrosis, but also different liver metabolic capacity. As the degree of fibrosis increases, the fibrotic liver gradually deteriorated and could not effectively clear polymeric nanoparticles. The activation and proliferation of HSCs improved polymeric nanoparticle binding efficiency, while the increase of collagen content reduced the permeability of polymeric particles. In order to investigate the targeting and distribution, free DiR, HA@DiR NPs, and HA@DiR/COL NPs were injected into normal mice or mice treated with CCl₄ for 8 weeks via the tail vein and measured near infrared fluorescence emission by employing *in vivo* small animal imaging system. As shown in Fig. 7B and 7D, polymeric nanoparticles of normal mice group in the liver reached a peak at 24 h and then declined, which is mainly due to the rapid decline in normal liver metabolic capacity. Contrarily, the fluorescence intensity of all types of polymeric nanoparticles maintained at higher levels for 6 h to 5 d in the liver region of the fibrotic mice, which might be a result of liver dysfunction and collagen deposition in the Diss space (Fig. 7C and 7E).

The liver, spleen, kidney, lung, and heart were harvested on day 5 after injection, and *ex vivo* imaging was used to assess fluorescence emission. According to the organ fluorescence data shown in Figure S11 and S12, the livers of mice with fibrotic livers and normal livers fluoresced much more than other tissues. Furthermore, compared to free DiR and HA@DiR NPs, HA@DiR/COL

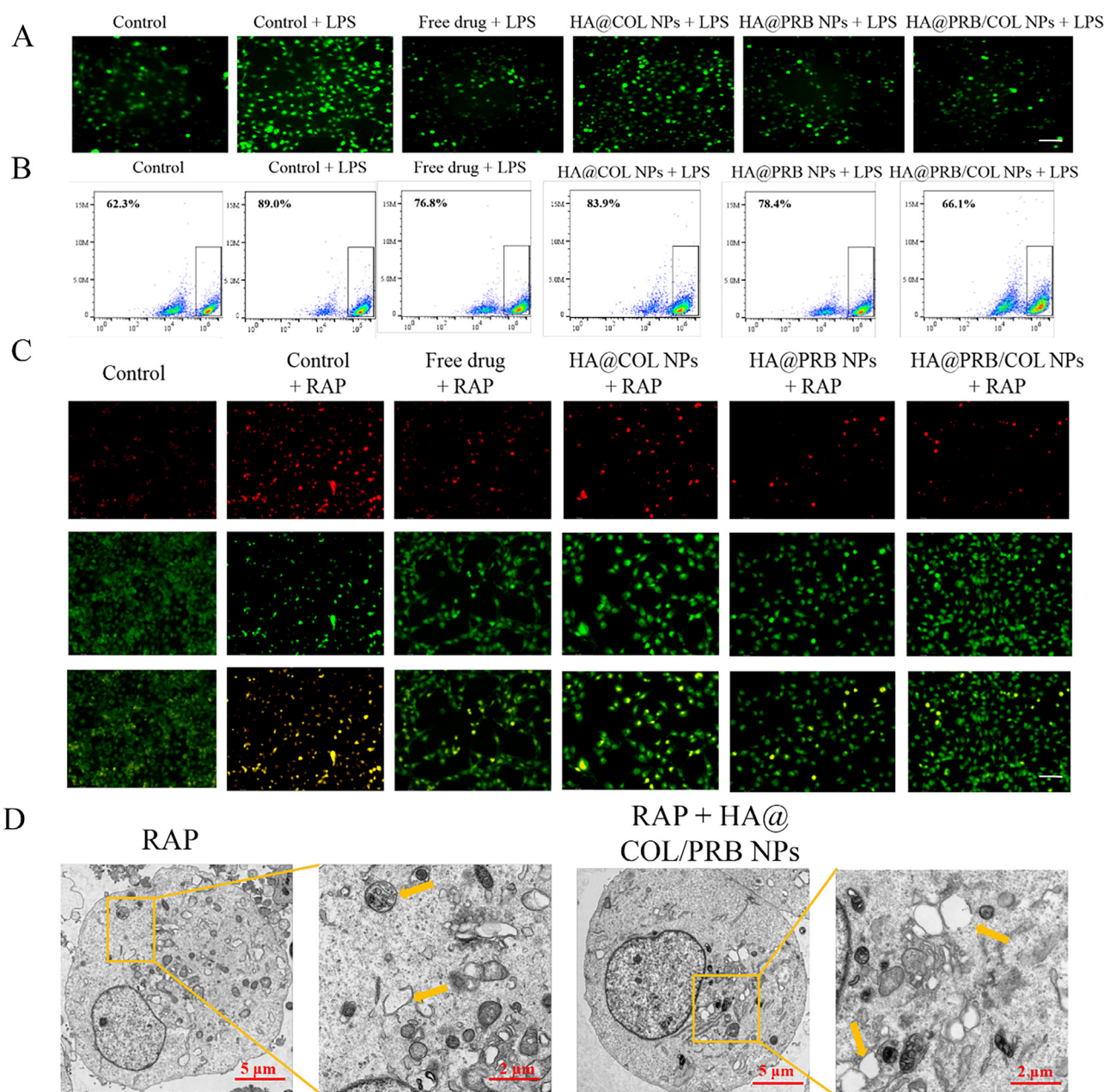


Fig. 6. HA@PRB/COL NPs inhibits the activation of LX2 by ROS reduction and inhibiting autophagy. (A) CLSM of the removal of ROS after different treatments were measured by DCFH-DA. Scale bar = 100 μ m. (B) Flow cytometry analysis of the removal of ROS after different treatments were measured by DCFH-DA. (C) CLSM images of AO staining of LX2 cells after different treatment. Scale bar = 100 μ m. (D) Bio-TEM of formation and destruction of autophagosomes.

NPs produced stronger signals in the liver of fibrotic and normal mice.

3.8. ECM degradation and activated HSCs targeting efficiency in vivo

The constructed polymer nano-delivery system is anticipated to eventually target liver-based activated HSCs. We loaded different polymeric nanoparticles with the FITC and then intravenously administered FITC-labeled polymeric nanoparticles to normal mice or liver fibrosis model mice treated with CCl_4 for 8 weeks to further demonstrate the targeting and penetration ability of polymeric nanoparticles. As displayed in Fig. 8A and 8B, mice injected with HA@FITC/COL NPs, as opposed to free FITC and HA@FITC NPs, green FITC fluorescence fused heavily with the Cy3-labeled α -SMA (red signal) of the liver, producing a strong yellow signal, indicating that

the majority of FITC was located in activated HSCs in HA@FITC/COL NPs treatment group. Together, these results clearly shown that collagenase type I (COL) contributed to deeper penetration of the ECM barrier. This property of HA@FITC/COL NPs nanocarriers had been shown to facilitate efficient delivery in fibrotic liver.

To further demonstrated that HA@FITC/COL NPs selectively targeted activated HSCs through the CD44 receptor-mediated endocytosis pathway, immunofluorescence staining of CD44 receptors in the fibrotic liver was performed. In contrast to free FITC and the HA@FITC NPs group in fibrotic liver, the green FITC fluorescence of HA@FITC/COL NPs group was observed to have mainly blended with the red fluorescence of HSCs, resulting in an intense yellow signal (Fig. 8D), the majority of FITC was detected in activated HSCs in the HA@FITC/COL NPs group (Fig. 8E). However, if the CD44 receptor on the surface of the activated HSCs was initially pre-

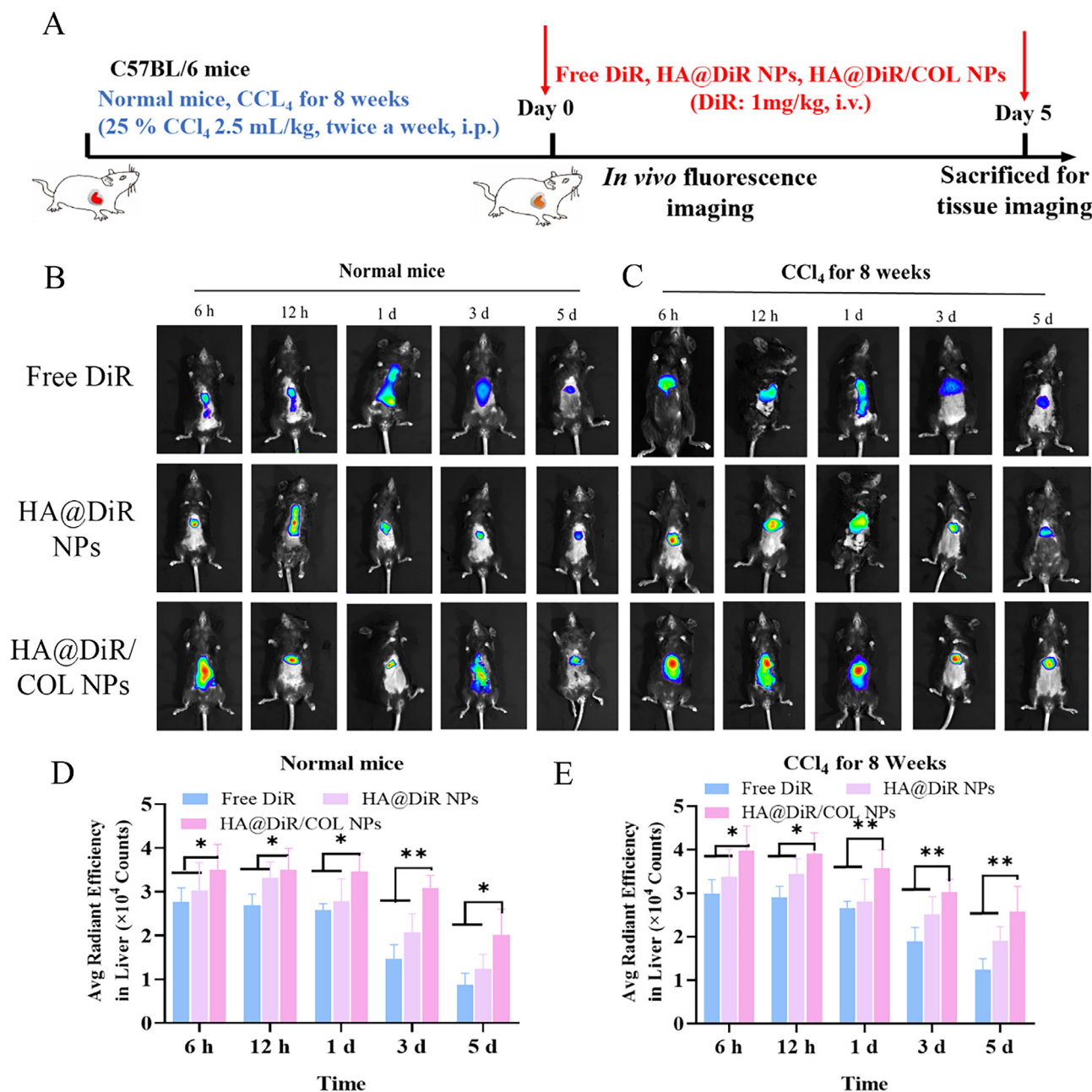


Fig. 7. Distribution of DiR-loaded polymeric nanoparticles in normal and fibrotic mice. (A) Schematic summary of animal studies. Representative *in vivo* fluorescence imaging system images of normal mice (B) and mice treated with CCl₄ for 8 weeks (C) acquired at different time points after intravenous injection with different formulations. Fluorescence intensity in normal mice (D) and mice treated with CCl₄ for 8 weeks (E). Values are expressed as means \pm SD (error bars; * p < 0.05, ** p < 0.01, n = 3).

saturated with HA solution and the overlapping yellow signal was comparatively faint in the HA@FITC/COL NPs, demonstrating that the CD44 receptor was the main internalizing pathway for activated HSCs. These results further validated that systematic administration of HA@PRB/COL NPs could target activated HSCs *in vivo* and deliver biomacromolecules and chemotherapy drugs into cells to treat hepatic fibrosis.

The faint immunofluorescence signals for α -SMA and CD44 in the livers of normal mice are depicted in Fig. 8A and 8D, suggesting the inactivation of HSCs. In addition, the fluorescence intensity of HA@FITC/COL NPs was significantly lower in normal liver (Fig. 8C and 8F), the main reason was that the activation and proliferation of HSCs in liver fibrosis enhanced the binding sites, and the decreased clearance of fibrotic liver led to the accumulation of HA@FITC/COL NPs in the liver.

3.9. Antifibrotic activity of HA@PRB/COL NPs *in vivo*

The delivery of PRB and COL to HSCs for treating hepatic fibrosis is the goal of nano-delivery system construction. We investigated the *in vivo* antifibrotic activity of HA@PRB/COL NPs using the mice with fibrotic liver, and we administered different polymeric nanoparticles formulations to mice twice weekly for three weeks, and evaluated therapeutic efficacy at third day after the last treatment (Fig. 9A). Liver tissue was excised and imaged after dissection. The degree of liver fibrosis in the model group was significantly increased, and the liver fibrosis in the drug treatment group was recovered to varying degrees (Figure.S13). As shown in Fig. 8B and 8C, HA@PRB/COL NPs group could alleviate liver fibrosis in mice model by inhibiting autophagy. Hepatic fibrosis impairs normal liver function, so levels of alanine aminotransferase

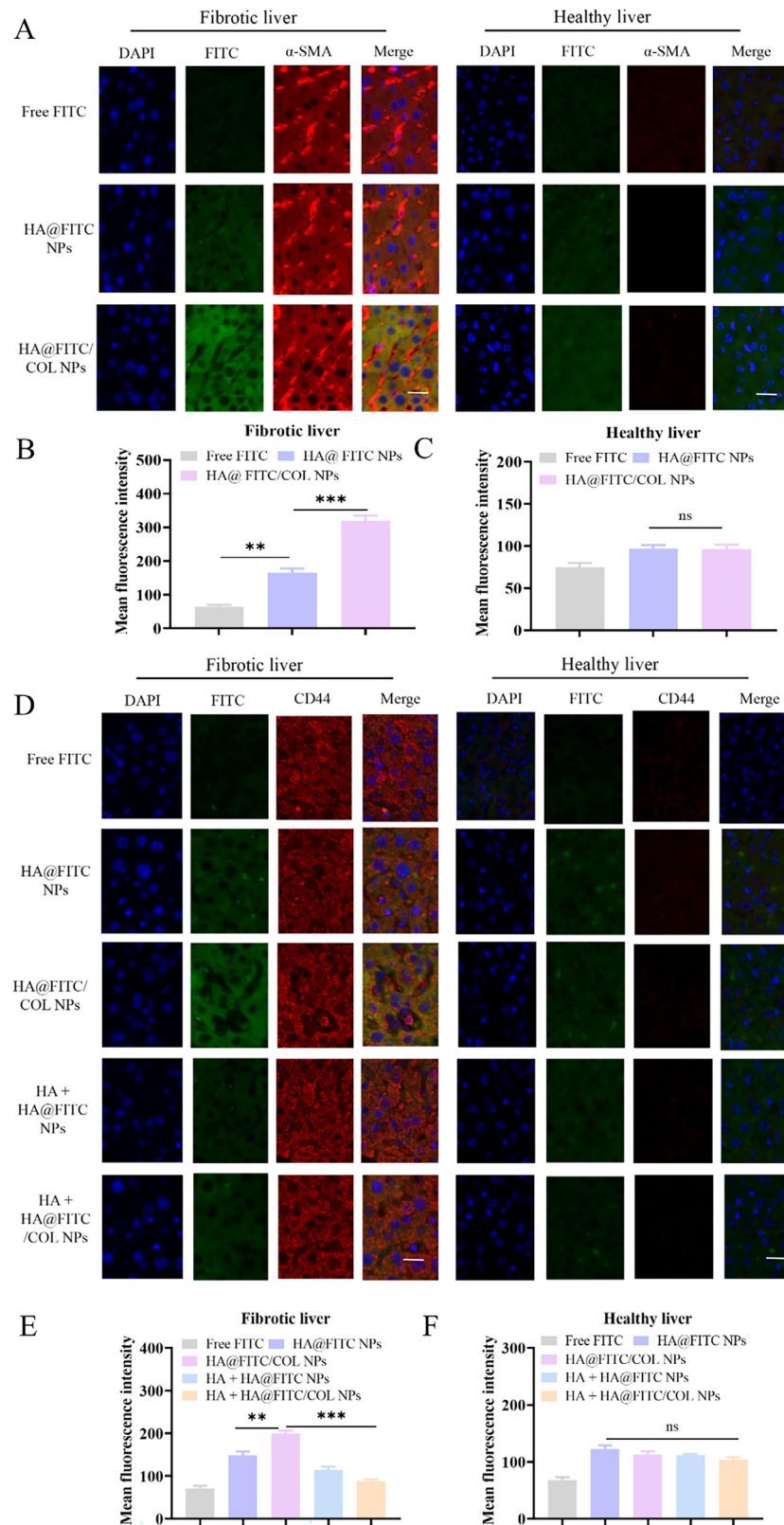


Fig. 8. Co-localization of FITC and FITC-labeled polymeric nanoparticles with activated HSCs in the livers of fibrotic mice treated with CCl_4 for 8 weeks. (A) Liver tissue was sectioned and immune-stained with an anti- α -SMA antibody (red) for activated HSCs and counterstained with the nuclear dye, DAPI (blue). (B) and (C) Mean fluorescence intensity of FITC in fibrotic liver tissue and healthy liver tissue immune-stained with an anti- α -SMA antibody. (D) Liver tissue was sectioned and immune-stained with an anti-CD44 antibody (red) for activated HSCs and counterstained with the nuclear dye, DAPI (blue). (E) and (F) Mean fluorescence intensity of FITC in fibrotic liver and healthy liver tissue immune-stained with an anti-CD44 antibody. Co-localization was determined as yellow signals corresponding to perfect merges of green and red fluorescence. After polymeric nanoparticles were injected into HA pre-saturated mice, HSCs were labeled with CD44 antibody and the distribution of polymeric nanoparticles was observed in liver tissue. Scale bar = 50 μm . $**p < 0.01$, $***p < 0.001$; ns, no significant difference ($n = 3$, mean \pm SD).

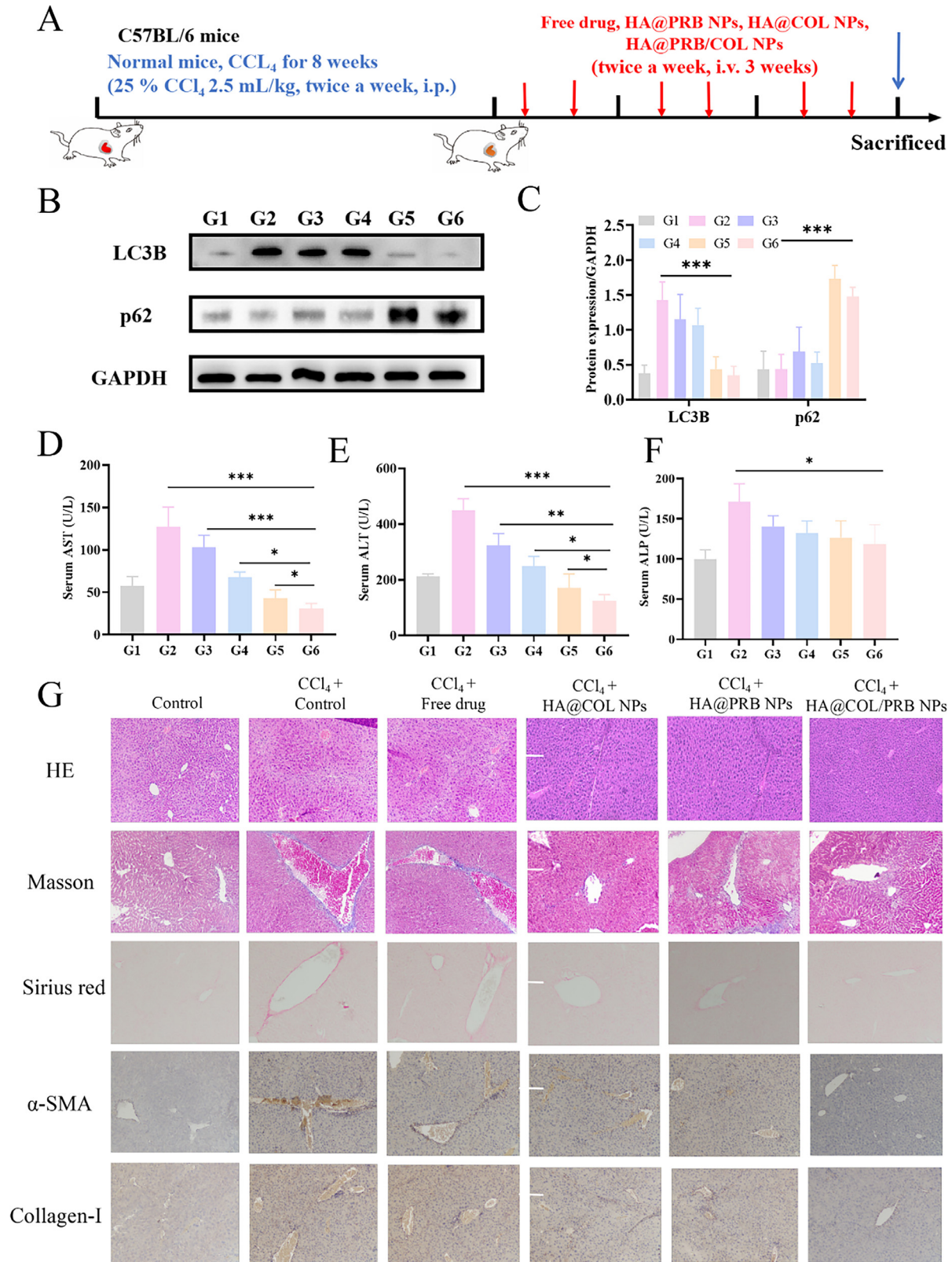


Fig. 9. Antifibrotic activity of HA@PRB/COL NPs *in vivo*. (A) Schematic diagram of anti-liver fibrosis efficacy study *in vivo*. (B) and (C) The protein expressions of LC3B, and p62 were assayed by western blot, GAPDH was included as loading control. Liver function as indicated by serum levels of AST (D), ALT (E) and ALP (F). (G) H&E, Masson, Sirius red staining and immunohistochemical staining of α -SMA and collagen I in livers of fibrotic mice after treatment with different formulations. Scale bar = 50 μ m. G1: control, G2: CCL₄ + control, G3: CCL₄ + free drug, G4: CCL₄ + HA@COL NPs, G5: CCL₄ + HA@PRB NPs, G6: CCL₄ + HA@PRB/COL NPs. **p* < 0.05, ***p* < 0.01, ****p* < 0.001, and ns means no significant difference (*n* = 5, mean \pm SD).

(ALT), aspartate aminotransferase (AST), and alkaline phosphatase (ALP) are used to assess liver function damage. The levels of serum ALT, AST, and ALP in mice receiving various treatments were suggested to vary in Fig. 9D-F. CCl₄ significantly elevated AST and ALT, whereas serum levels of AST and ALT were definitely decreased to a larger extent in fibrotic mice given free drug (G3), HA@COL NPs (G4), HA@PRB NPs (G5), or HA@PRB/COL NPs (G6) than in mice given PBS. As shown in Figure.S14, hydroxyproline (Hyp) content (a major component of collagen) of HA@PRB/COL NPs-treated fibrotic mice showed significantly decrease, indicating that the Hyp generation was suppressed. Notably, AST and ALT levels were nearly normal in the mice treated with HA@PRB/COL NPs, showing that the drug delivery effectiveness of COL modification and better HSCs targeting increased the therapeutic effect of hepatic fibrosis.

In addition to biochemical testing, semi-quantitative immunohistochemistry was used to assess the combination therapeutic effectiveness of HA@PRB/COL NPs. In contrast to the livers of healthy mice, the PBS-treated group displayed symptoms of fibrous connective tissue hyperplasia, inflammatory cell infiltration, or fibrous tissue hyperplasia, as seen in Fig. 9G. This inflammatory response was alleviated to varying degrees by treatment with free drug, HA@PRB NPs, HA@COL NPs and HA@PRB/COL NPs. CCl₄-induced mice treated with HA@PRB/COL NPs showed significantly reduced levels of HSCs activation and hepatic collagen accumulation according to Masson trichromatic staining and Sirius red staining (Fig. 9G). Further, semi-quantitative assays of Masson trichromatic staining and Sirius red staining of dissected liver tissues also indicated that HA@PRB/COL NPs treatment group resulted in a significant reduction in collagen area and fibrous tissues were repaired (Figure.S15). Additionally, immunohistochemical studies revealed that the CCl₄-induced mice treated with HA@PRB/COL NPs had decreased levels of collagen I and α -SMA expression, suggesting that the process of liver fibrosis could be stopped by blocking the activation of HSCs (Figure.S16). In addition, mice treated with all formulations demonstrated that there were few abnormalities observed in histological sections of the heart, spleen, lung, or kidney tissue. The targeting delivery led to increased accumulation of PRB in the liver, and the incidence of adverse reactions might decrease. According to the safety evaluation findings suggested that HA@PRB/COL NPs displayed good long-term biosafety (Figure.S17).

In general, we evaluated hepatic fibrosis by a variety of methods, including immunohistochemical staining, hydroxyproline content measurement and examination of serum AST, ALT and ALP levels to assess liver function. The results showed that HA@PRB/COL NPs could significantly improve the pathological environment of the liver, repair most of the fibrosis, reduce the number of activated HSCs, and basically restore the liver cell morphology to the normal level. Taken together, it concluded that the synergistic effect of HA@PRB/COL NPs had a stronger ability to repair fibrous tissues and better delivery efficiency.

4. Conclusions

Current nanomedical delivery systems targeting HSCs for hepatic fibrosis are difficult to reach the liver due to the excessive deposition of fibrotic collagen. In this project, we designed a COL-modified nano-codelivery system, which could penetrate the excess collagen barrier of fibrotic liver and ultimately achieve efficient targeting of HSCs. The construction of HA@PRB/COL NPs effectively degraded and penetrated fibrotic ECM in the fibrotic liver owing to the proteolysis function of collagenase type I, then the HA@PRB/COL NPs were internalized by the HSCs via the CD44 receptors mediated endocytosis pathway through the surface coated HA, and finally PRB was released continuously in the cells. *In vitro* and *in vivo* experiments showed that HA@PRB/COL NPs exhibited the ability to ameliorate hepatic fibrosis by degrading

the fibrotic ECM and inhibiting HSCs activation and proliferation. More important, we also demonstrated that HA@PRB/COL NPs have good cytocompatibility and hemocompatibility *in vitro* and has no acute or chronic toxicity *in vivo*. Based on the above findings, our HA@PRB/COL NPs system is an ideal HSCs-targeting, convenient nano-drug delivery system to combine biomacromolecular and small-molecule drugs for hepatic fibrosis therapy. HA@PRB/COL NPs system demonstrated that collagenase I modified nanocarrier might be a new strategy for the design of more effective therapeutic vectors targeting liver fibrosis.

Declaration of Competing Interest

The authors declare that they have no competing interest.

Acknowledgments

This study was supported by National Natural Science Foundation of China (NSFC) [81571213 and 82070459 (Bin Wang)], Key Project of Jiangsu Province (Grant No. BE2020765) (Bin Wang), and Project of Modern Hospital Management and Development Institute, Nanjing University/Aid project of Nanjing Drum Tower Hospital Health, Education & Research Foundation (NDYG2020030) (Bin Wang). Jiangsu Biobank of Clinical Resources (BM2015004).

Supplementary materials

Supplementary material associated with this article can be found, in the online version, at doi:10.1016/j.actbio.2023.12.027.

References

- [1] R Bataller, DA Brenne, Liver fibrosis, *J. Clin. Invest.* 115 (2) (2015) 209–218.
- [2] G Garcia-Tsao, J. Lim, Management and treatment of patients with cirrhosis and portal hypertension: recommendations from the department of veterans affairs hepatitis C resource center program and the national hepatitis C program, *Am. J. Gastroenterol.* 104 (7) (2009) 1802.
- [3] Duan Jinzhu, Ghergh Costin, Liu Dianxin, Hamlett Eric, Srikantha Luxman, Rodgers Laurel, Regan Jenna N, Rojas Mauricio, Willis Monte, Leask Andrew, Majesky Mark, Deb Arjun, Wnt1/ β -catenin injury response activates the epicardium and cardiac fibroblasts to promote cardiac repair, *EMBO J.* 31 (2) (2012) 429–442.
- [4] Henderson William R, Chi Emil Y, Ye Xin, Nguyen Cu, Tien Ying-tzang, Zhou Beiyun, Borok Zea, Knight Darryl A, Kahn Michael, Inhibition of Wnt/ β -catenin/CREB binding protein (CBP) signaling reverses pulmonary fibrosis, *Proc. Natl. Acad. Sci. U. S. A.* 107 (32) (2010) 14309–14314.
- [5] Kim Yuhree, Ejaz Aslam, Tayal Amit, Spolverato Gaya, F.P Bridges John, A Anders Robert, M Pawlik Timothy, Temporal trends in population-based death rates associated with chronic liver disease and liver cancer in the United States over the last 30 years, *Cancer* 120 (19) (2014) 3058–3065.
- [6] Y.A. Lee, M.C. Wallace, S.L. Friedman, Pathobiology of liver fibrosis: a translational success story, *Gut* 64 (2015) 830–841.
- [7] A. Pellicoro, P. Ramachandran, J.P. Iredale, J.A. Fallowfield, Liver fibrosis and repair: immune regulation of wound healing in a solid organ, *Nat. Rev. Immunol.* 14 (2014) 181–194.
- [8] F. Li, Y. Qiu, F. Xia, H. Sun, H. Liao, A. Xie, J. Lee, P. Lin, M. Wei, Y. Shao, B. Yang, Q. Weng, D. Ling, Dual detoxification and inflammatory regulation by ceria nanozymes for drug-induced liver injury therapy, *Nano Today* 35 (2020) 100925.
- [9] X.W. Zhang, J.C. Zhou, D. Peng, F. Hua, K. Li, J.J. Yu, X.X. Lv, B. Cui, S.S. Liu, J.M. Yu, F. Wang, C.C. Jin, Z.N. Yang, C.X. Zhao, X.Y. Hou, B. Huang, Z.W. Hu, Disrupting the TRIB3-SQSTM1 interaction reduces liver fibrosis by restoring autophagy and suppressing exosome-mediated HSC activation, *Autophagy* 16 (2020) 782–796.
- [10] H.M. Ni, X. Chao, H. Yang, F. Deng, S. Wang, Q.Y. Bai, Cui Y Qian, W. Cui, Y.H. Shi, W.X. Zong, Z.T. Wang, L. Yang, W.X. Ding, Dual roles of mammalian target of rapamycin in regulating liver injury and tumorigenesis in autophagy-defective mouse liver, *Hepatology* 70 (2019) 2142–2155.
- [11] R. Yang, Z. Hu, P. Zhang, S. Wu, Z. Song, X. Shen, Z. Wei, Probuco ameliates hepatic stellate cell activation and autophagy is associated with farnesoid X receptor, *J. Pharmacol. Sci.* 139 (2019) 120–12.
- [12] Bergmann Christina, Akhmetshina Aliya, Dees Clara, Palumbo Katrin, Zerr Pawel, Beyer Christian, Zwerina Jochen, Distler Oliver, Schett Georg, Distler Jörg H W. Inhibition of glycogen synthase kinase 3 β induces dermal fibrosis by activation of the canonical Wnt pathway, *Ann. Rheum. Dis.* 70 (12) (2011) 2191–2198.

- [13] Jason H Cheng, Hongyun She, Yuan-Ping Han, Jiaohong Wang, Shigang Xiong, Kinji Asahina, Hidekazu Tsukamoto, Wnt antagonism inhibits hepatostellate cell activation and liver fibrosis, *Am. J. Physiol. Gastrointest. Liver Physiol.* 294 (2008) G39–G49.
- [14] X.L. Zhang, Z.N. Chen, Q.F. Huang, F.C. Bai, J.L. Nie, S.J. Lu, J.B. Wei, X. Lin, Methyl helicterate inhibits hepatic stellate cell activation through modulation of apoptosis and autophagy, *Cell. Physiol. Biochem.* 51 (2018) 897–908.
- [15] YD Wang, WD Chen, M Wang, D Yu, BM Forman, W. Huang, Farnesoid X receptor antagonizes nuclear factor kappaB in hepatic inflammatory response, *Hepatology* 48 (5) (2008) 1632–1643.
- [16] L. Lin, H. Gong, R. Li, J. Huang, M. Cai, T. Lan, W. Huang, Y. Guo, Z. Zhou, Y. An, Z. Chen, L. Liang, Y. Wang, X. Shuai, K. Zhu, Nanodrug with ROS and pH dual-sensitivity ameliorates liver fibrosis via multicellular regulation, *Adv. Sci.* 7 (2020) 1903138.
- [17] Ajoolabady Amir, Aghanejad Ayuob, Bi Yaguang, Zhang Yingmei, Askhodapasandhukmabad Hamid, Abhari Alireza, Ren Jun, Enzyme-based autophagy in anti-neoplastic management: From molecular mechanisms to clinical therapeutics, *Biochim. Biophys. Acta Rev. Cancer* 1874 (1) (2020) 188366.
- [18] S.L. Friedman, Liver fibrosis – From bench to bedside, *J. Hepatol.* 38 (2003) 38–53.
- [19] P.P. Provenzano, C Cuevas, A.E. Chang, V.K. Goel, D.D. Von Hoff, S.R. Hingorani, Enzymatic targeting of the stroma ablates physical barriers to treatment of pancreatic ductal adenocarcinoma, *Cancer Cell* 21 (3) (2012) 418–429.
- [20] T. Higashi, S.L. Friedman, Y. Hoshida, Hepatic stellate cells as key target in liver fibrosis, *Adv. Drug Deliv. Rev.* 121 (2017) 27–42.
- [21] A. Khanam, P. Saleeb, S. Kottilil, Pathophysiology and treatment options for hepatic fibrosis: can it be completely cured? *Cells* 10 (5) (2021) 1097.
- [22] Y. Zhang, W. Poon, A. Tavares, I. McGilvray, W. Chan, Nanoparticle-liver interactions: Cellular uptake and hepatobiliary elimination, *J. Control. Release.* 240 (2016) 332.
- [23] C.Y. Zhang, W.G. Yuan, P. He, J.H. Lei, C.X. Wang, Liver fibrosis and hepatic stellate cells: etiology, pathological hallmarks and therapeutic targets, *World J. Gastroenterol.* 22 (2016) 10512–10522.
- [24] W. Li, C. Zhou, Y. Fu, T. Chen, X. Liu, Z. Zhang, T. Gong, Targeted delivery of hyaluronic acid nanomicelles to hepatic stellate cells in hepatic fibrosis rats, *Acta Pharmaceutica Sinica B* 10 (4) (2020) 693–710.
- [25] D. Ossipov, Hyaluronan-based delivery of therapeutic oligonucleotides for treatment of human diseases, *Expert. Opin. Drug. Del.* 16 (6) (2019) 621–637.
- [26] W. Li, C. Zhou, Y. Fu, T. Chen, X. Liu, Z. Zhang, T. Gong, Targeted delivery of hyaluronic acid nanomicelles to hepatic stellate cells in hepatic fibrosis rats, *Acta. Pharm. Sin. B.* 10 (4) (2020) 693–710.
- [27] K. Park, S. Hong, W. Hur, M. Lee, J.Y. ang, S. Kim, S.Y. oon, S. Hahn, Target specific systemic delivery of TGF- β siRNA/(PEI-SS)-g-HA complex for the treatment of liver cirrhosis, *Biomaterials* 32 (21) (2011) 4951–4958.
- [28] M. Villegas, A. Baeza, M. Vallet-Regí, Hybrid collagenase nanocapsules for enhanced nanocarrier penetration in tumoral tissues, *ACS. Appl. Mater. Inter.* 7 (43) (2015) 24075–24081.
- [29] J. Li, C. Xie, J. Huang, Y. Jiang, Q. Miao, K. Pu, Semiconducting polymer nanoenzymes with photothermal activity for enhanced cancer therapy, *Angewandte Chemie* 57 (15) (2018) 3995–3998.
- [30] Q. Fan, C. Zhang, J. Qiao, P. Cui, L. Xing, Y. Oh, H. Jiang, Extracellular matrixpenetrating nanodril micelles for liver fibrosis therapy, *Biomaterials* 230 (2020) 119616.
- [31] E. Geervliet, S. Moreno, L. Baiaomonte, R. Booiink, S. Boye, P. Wang, B. Voit, A. Lederer, D. Appelhans, R. Bansal, Matrix metalloproteinase-1 decorated polymersomes, a surface-active extracellular matrix therapeutic, potentiates collagen degradation and attenuates early liver fibrosis, *J. Control. Release.* 332 (2021) 594–607.
- [32] Fan Qian-Qian, Zhang Cheng-Lu, Qiao Jian-Bin, Cui Peng-Fei, Xing Lei, Oh Yu-Kyoung, Jiang Hu-Lin, Extracellular matrix-penetrating nanodril micelles for liver fibrosis therapy, *Biomaterials* 230 (2020) 119616.
- [33] Colak Yasar, Senates Ebubekir, Coskuncinar Ender, Oltulu Yasemin Musteri, Zemheri Ebru, Ozturk Oguzhan, Doganay Levent, Mesci Banu, Yilmaz Yusuf, Enc Feruze Yilmaz, Kiziltas Safak, Ulasoglu Celal, Ilyas Tuncer, Concentrations of connective tissue growth factor in patients with nonalcoholic fatty liver disease: association with liver fibrosis, *Dis. Markers* 33 (2) (2012) 77–83.
- [34] Piao Rong-Li, Brigstock David R, Zhu Jie, Zhang Man-Li, Gao Run-Ping, Clinical significance of connective tissue growth factor in hepatitis B virus-induced hepatic fibrosis, *World J. Gastroenterol.* 18 (18) (2012) 2280–2286.
- [35] J. Moscat, M.T. Diaz-Meco, p62 at the crossroads of autophagy, apoptosis, and cancer, *Cell* 137 (2009) 1001–1004.
- [36] F. Tanabe, K. Yone, N. Kawabata, H. Sakakima, F. Matsuda, Y. Ishidou, S. Maeda, M. Abematsu, S. Komiya, T. Setoguchi, Accumulation of p62 in degenerated spinal cord under chronic mechanical compression: functional analysis of p62 and autophagy in hypoxic neuronal cells, *Autophagy* 7 (2011) 1462–1471.